BNL-216333-2020-JAAM

Perovskite Solar Cells with Enhanced Fill Factors Using Polymer-Capped Solvent Annealing

J. Kong, M. Cotlet

To be published in "ACS Applied Energy Materials"

July 2020

Center for Functional Nanomaterials

Brookhaven National Laboratory

U.S. Department of Energy

USDOE Office of Science (SC), Basic Energy Sciences (BES) (SC-22)

Notice: This manuscript has been authored by employees of Brookhaven Science Associates, LLC under Contract No. DE-SC0012704 with the U.S. Department of Energy. The publisher by accepting the manuscript for publication acknowledges that the United States Government retains a non-exclusive, paid-up, irrevocable, world-wide license to publish or reproduce the published form of this manuscript, or allow others to do so, for United States Government purposes.

DISCLAIMER

This report was prepared as an account of work sponsored by an agency of the United States Government. Neither the United States Government nor any agency thereof, nor any of their employees, nor any of their contractors, subcontractors, or their employees, makes any warranty, express or implied, or assumes any legal liability or responsibility for the accuracy, completeness, or any third party's use or the results of such use of any information, apparatus, product, or process disclosed, or represents that its use would not infringe privately owned rights. Reference herein to any specific commercial product, process, or service by trade name, trademark, manufacturer, or otherwise, does not necessarily constitute or imply its endorsement, recommendation, or favoring by the United States Government or any agency thereof or its contractors or subcontractors. The views and opinions of authors expressed herein do not necessarily state or reflect those of the United States Government or any agency thereof.

Perovskite Solar Cells with Enhanced Fill Factors Using Polymer-Capped Solvent Annealing

Jaemin Kong, Hanyu Wang, Jason A. Röhr, Zachary S. Fishman, Yuanyuan Zhou, Mingxing Li, Mircea Cotlet, Geunjin Kim, Christopher Karpovich, Francisco Antonio, Nitin P. Padture, and André D. Taylor*

ABSTRACT: Despite huge improvements in power conversion efficiencies of perovskite solar cells, the technology is still limited by fill factors at around 80%. Here, we report perovskite solar cells having exceptionally high fill factors of 85% and enhanced open-circuit voltage without sacrificing short-circuit current through a polymer-capped solvent-annealing process assisted by a hot air blower. During the solvent-annealing, the perovskite surface flattens and the perovskite grains agglomerate into micrometer-sized clusters having enlarged α-phase crystallites, while the δ-phase simultaneously disappears. The optimized structure reduces energetic disorder and trap-assisted recombination in the perovskite layer, resulting in an enhanced efficiency from 18.2% to 19.8% and improved device lifetime. Our results provide a pathway to increase the device efficiency and stability of perovskite solar cells, and have the potential to stimulate research on scalable polycrystal perovskite layer fabrication in optoelectronic devices.

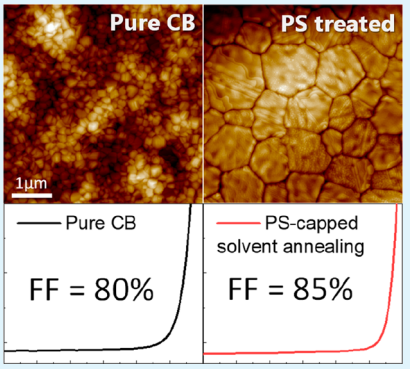

KEYWORDS: *perovskite solar cells, large clusters, polymer-capped solvent annealing, hot air blower, high fill factor*

Organic−inorganic metal halide perovskite solar cells have received great attention due to their excellent optoelectronic properties including a large absorption coefficient (~10^5 cm^{-1}),[1] a low exciton binding energy (~20 meV),[2] and a relatively long charge-carrier diffusion length (~1 μm),[3] and have shown dramatic improvements in the power conversion efficiency (PCE) from 3.8% to a certified 25.2% over the past few years.[4] On the basis of the Shockley−Queisser limit, a theoretical PCE limit for E_g of ~1.6 eV is approximately 30% with a short-circuit current density (J_{SC}) of ~25 mA cm^{-2}, open-circuit voltage (V_{OC}) of ~1.3 V, and fill factor (FF) of ~90%.[5−7] With record cells having a J_{SC} of ca. 24 mA cm^{-2}, a V_{OC} of 1.10−1.16 V, and a FF of 73−81%,[8−10] there is still room for PCE improvement if the parameters such as V_{OC} and FF could be further enhanced.

A feasible way to further enhance the solar cell parameters is to reduce defects in the solar cells.[11,12] In a polycrystalline perovskite layer, defects and/or halide segregations, which act as trap/recombination centers, are typically concentrated at grain boundaries and interfaces.[13] Bi et al. achieved an enhanced V_{OC} of 1.16 V with a high J_{SC} of 24.6 mA cm^{-2} by adding an excess of lead iodide (PbI_2) which induced the growth of bigger perovskite grains/crystallites.[8] Enlarging the crystallite size and reducing the area of grain boundaries lowered the trap density of the perovskite layer, giving rise to a higher V_{OC}; however, the FF of the solar cell still exhibited a relatively low value of 73%. Although the excessive PbI_2 can be used as seeds to grow bigger perovskite crystallites, the excess of PbI_2 might give rise to additional defects such as nonstoichiometric lattice disorder in the grains or halide segregation at the grain boundaries. Recently, Yang et al. reported an internal passivation method to reduce compositional point defects (i.e., I-deficient intermediates) that are charge-balanced by positive ions in the perovskite layer. By introducing additional triiodide ions, deep-level traps were significantly reduced while the proportion of α-$FAPbI_3$ phases in the resulting layer increased, which led to an enhanced FF of 81.9%.[9] Although the deep-level traps were removed with the aid of additional triiodide ions, the V_{OC} was still limited at ~1.1 V. This may originate from another defect source, for example, iodine interstitials or iodine enrichment at grain boundaries, resulting in a reduced band gap.[14]

Another strategy to reduce defects in the perovskite solar cells has been sought by employing polymers or small molecules in the antisolvents during a perovskite film fabrication process.[15−18] By dripping polymer (or small molecule) solutions, instead of pure organic solvents, inner passivation layers have been formed between perovskite and hole transporting layers,

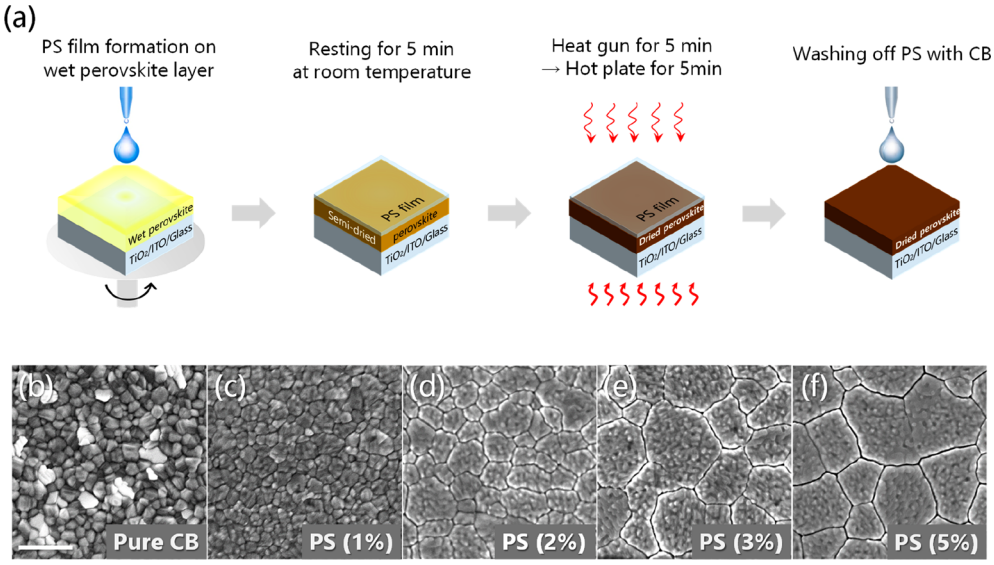

Figure 1. (a) Schematic of the polymer-capped solvent-annealing process during perovskite layer fabrication. Top-view SEM images of perovskite films fabricated using (b) pure CB, and PS solutions: (c) 1% PS solution, (d) 2% PS solution, (e) 3% PS solution, and (f) 5% PS solution, respectively. Prior to the SEM observations, the PS polymer layers were completely removed by multiple rinsings with CB solvent. The scale bar is 1 μm.

which could reduce interfacial defects. Moreover, the thin organic layers could act as templates for nucleation and crystal growth of perovskite layers. In previous studies, diluted solutions, below 10 mg mL^{-1}, were employed as the polymer layers were also intended to be used as inner passivation layers; if the organic layers are too thick, regardless of their band gaps and energy levels, they had a deterimental effect on charge transport and collection.[19] The role of high concentrations of organic solutions, leading to thicker organic films, on perovskite layer formations has therefore been overlooked.

Here, we demonstrate that a high concentration of polystyrene solution could lead to larger clustered grains with the size of a few micrometers in the perovskite layer, resulting in exceptionally high FF of 85% and V_{OC} of ~1.15 V (without sacrificing J_{SC}). A hot air blower enables the thick top polymer film to be dried prior to the underlying still-wet perovskite layer, giving a time for perovskite grains to grow along with the flat dried polymer film. Moreover, the dried polymer film retards the solvent vaporization of the semidried perovskite layer in order for preformed perovskite gains to agglomerate to form larger clusters. This process also reduces the occurrence of δ-phase, which helps minimize structural defects in the perovskite layer. A simple rinsing step using a common organic solvent removes the polystyrene, ensuring that the insulating polystyrene film does not adversely affect charge transport and collection. The resulting perovskite layer possesses reduced energetic disorder and less trap-assisted recombination leading to enhanced efficiency and improved stability. Finally, we note that the significantly reduced surface roughness can provide a great platform for a large area solar cell manufacturing.

Figure 1a depicts a schematic of the polymer-capped solvent-annealing process and top-view SEM images of the perovskite layers processed with pure CB and CB containing 1, 2, 3, or 5 wt % polystyrene (PS), respectively. We found that 5 wt % is the highest polystyrene concentration we could employ before we started to experience drying issues where the PS films would tear during the hot air drying process. Although DMF and DMSO, which are the solvents for perovskite precursors, can permeate through the polystyrene films, we believe that thick polystyrene films will not allow for a rapid evaporation of DMF and DMSO during the drying process. During conventional processing of perovskite layers, pure chlorobenzene (CB) solvent is dripped during the spin-coating process of the perovskite solution on a TiO_2−Cl/ITO/glass substrate,[20,21] and the resultant film is shown in the SEM image (Figure 1b). However, during the polymer-capped solvent-annealing process, a PS solution is dripped while the perovskite solution coated substrate is spinning. During this polymer-coating process, a semidried PS film is formed onto a wet perovskite layer, which confines the perovskite solvents (DMF and DMSO) between the PS film and the bottom substrate since the PS film is almost neither soluble in DMF nor DMSO. After forming a thin layer of PS film on the wet perovskite layer, the substrate is kept in a N_2-glovebox at room temperature for 5 min. This method is akin to a conventional solvent-annealing process which has been widely used for organic solar cells to provide time to induce self-alignment of the organic molecules and to form higher crystallinities of the photoactive layer.[22,23] After the PS-capped solvent-annealing process, the samples were placed under a hot air blower to dry the PS film first from the top side. This drying process renders the underlying wet perovskite layer flat. If this heat gun step is skipped, we observe the formation of bumps and surface roughness on the perovskite layer (Supporting Information (SI) Figure S1a); for example, in the case of the 5% PS solution treatment directly followed by a hot plate annealing, the root-mean-square (RMS) roughness of the perovskite layer is as high as 64 nm, and the maximum roughness depth (R_{max}) reaches 494 nm, which is almost same length scale as the film thickness. Since both the PS and the perovskite layers are wet right after the polymer-coating process, it is reasonable to assume that the PS film will dry prior to the perovskite layer. The wet perovskite layer will for that reason dry along with the flat dried PS film surface. We also believe that the PS films will stiffen and flatten at a PS concentration of 3% or higher. In fact, we observe an increased roughness of the perovskite surface when low concentrations (0−2%) of PS are employed (Figure S1b−d). Beyond a PS concentration of 3%, the surface starts to flatten (Figure S1e,f). After drying the top

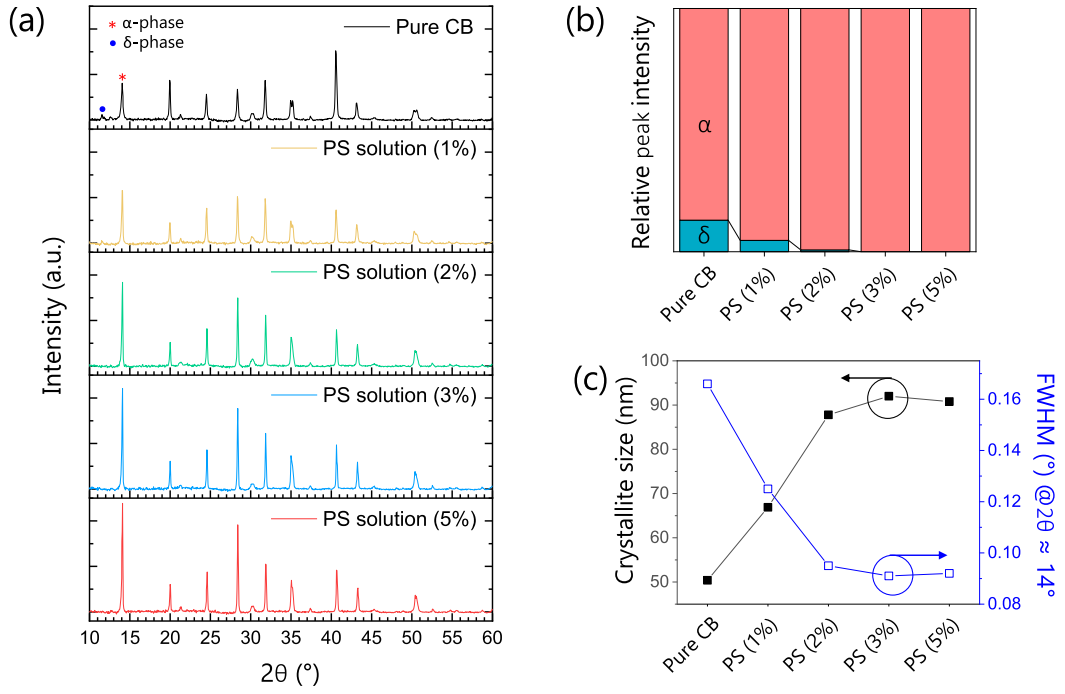

Figure 2. (a) XRD patterns of perovskite films with different concentrations of PS solutions. (b) Relative XRD peak intensities of α-phase and δ-phase crystallites in the perovskite films. The crystallite size was determined from the Scherrer equation. (c) Crystallite size and full width at half-maximum (fwhm) at $2\theta \approx 14°$ for each sample.

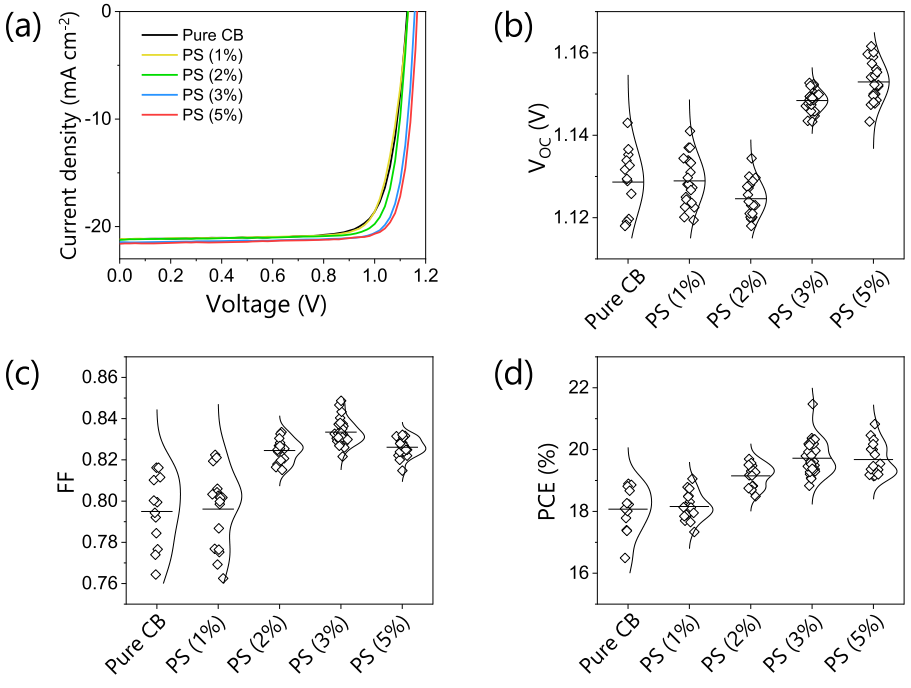

Figure 3. (a) Representative J–V curves, and measured data of (b) V_{OC}, (c) FF, and (d) PCE of the perovskite solar cells processed with pure CB and PS solutions with different concentration from 1 to 5%. Kernel smoothing functions were applied to more than 12 data points and were overlaid beside the data points to represent the data statistics.

PS film with a heat gun blower for 5 min, the substrate is moved onto a hot plate to completely dry all layers, including the perovskite layer. After the drying processes are completed, the top PS layer is removed by washing with CB. Using polarization modulation–infrared reflection absorption spectroscopy (PM-IRRAS), which has the advantage of high surface sensitivity, it was verified that no detectable PS remains on the perovskite film after washing (Figure S2). SEM images of the resultant perovskite films are shown in Figure 1c–f. Noticeably, beyond a 2% PS solution treatment (Figure 1d), the grains start clustering and the grain sizes increase to 1–2 μm, which is almost an order of magnitude larger than that of the control sample (Figure 1b). Moreover, the RMS roughness is significantly reduced from 17.7 to 10.1 nm, and the R_{max} also

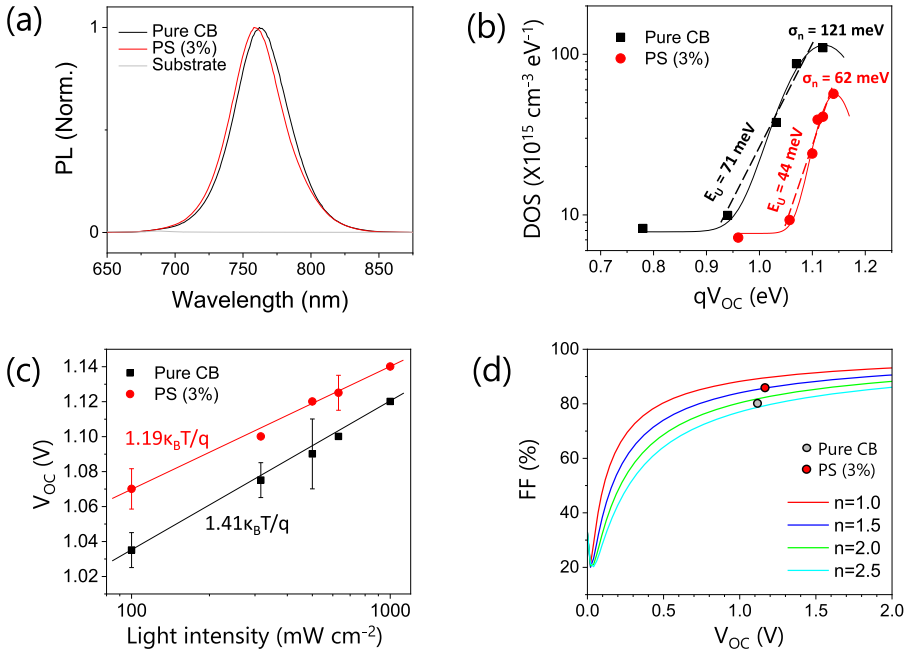

Figure 4. (a) Steady-state photoluminescence spectra of the films. Photoluminescence, (b) DOS of the devices and extracted parameters from a Gaussian or an Urbach tail fitting, (c) light intensity dependence of open-circuit voltage of the solar cells with and without polymer-capped solvent-annealing process, respectively, and (d) simulated curves with different ideality factors and the data points obtained from the solar cells with and without polymer-capped solvent annealing, respectively.

decreases from 138 to 85 nm when comparing a pure CB treated to the 5% PS solution treated perovskite film morphologies (Figure S1b–f).

To develop a deeper understanding of the changes in the microstructure resulting from the polymer-capped solvent-annealing processes, we studied XRD patterns of the treated perovskite layers (Figure 2a). From the XRD pattern for the control sample (pure CB), we observe a peak ($2\theta \approx 11.5°$) for photoinactive δ-$FAPbI_3$ phase (i.e., yellow phase).[24,25] However, as the PS concentration increases, the δ-phase peak reduces and finally disappears after 2% PS solution (Figure 2b). Converting from α- to δ-phase is energetically spontaneous and favorably occurs at the grain boundaries.[26,27] Since we brought the samples out of the N_2-glovebox for XRD measurement, the δ-phase might occur during the XRD measurement in air. Less grain boundaries in the concentrated PS-treated samples may reduce the probability of δ-phase occurrence in air. On the contrary, δ- to α-phase transformation needs energy, for example, a thermal energy by a hot plate.[28] Liu et al. recently reported that a large grain size in δ-phase intermediate films is essential for the growth of high-quality α-phase perovskite films.[28] Thus, the preformed large grains/clusters during the polymer-capped solvent-annealing process could favorably promote a growth of a high-quality α-phase perovskite layer. Indeed, we note that the photoactive α-phase peak centered at $2\theta \approx 14°$ significantly intensifies and the full width at half-maximum (fwhm) of the peak reduces dramatically, which reflects that the α-phase crystallites substantially grow from 50 to 90 nm as the PS solution concentration increases.[25]

To investigate the impact of the polymer-capped solvent annealing on the device performance, we fabricated solar cells using pure CB solvent and PS solutions with different concentrations (Figure 3a). Using up to 2% PS the V_{OC} slightly decreases, but above 2% PS the V_{OC} increases and reaches a maximum value of 1.16 V at 5% PS (Figure 3b). The slight V_{OC} reduction from 1.128 to 1.125 V might be attributed to the rough surface morphology of the perovskite layer (Figure S1d). The RMS and R_{max} increase from 17.7 to 30.5 nm and from 138 to 196 nm, respectively, when the PS concentration is increased from 0% to 2%. The rougher surface of the perovskite layer might cause an uneven thickness of the spiro-OMeTAD hole transporting layer on the rough perovskite layer surface. Since the R_{max} of the perovskite layer processed with 2% PS solution is 196 nm, the thickness of the Spiro-OMeTAD coated onto the ridges of the perovskite layer can be lower than that coated onto the flatter surface of the perovskite layer (Figure S3). This agrees with a recent study by Kim et al., who reported that when the thickness of the spiro-OMeTAD is below 180 nm, the V_{OC} of the solar cells shows a declining trend, while a thicker spiro-OMeTAD layer provides more reproducible performance.[29] In that work and elsewhere, however, the detailed mechanism on the correlation between thickness of spiro-OMeTAD and V_{OC} has not been elaborated. For a further understanding, in-depth studies need to be done in the future. As for the values for the FFs, a remarkable increase (FF ≈ 85%) was found employing the 3% PS solution with a narrower distribution of the FF (Figure 3c). Taken together, the polymer-capped solvent-annealing process enhanced the average PCE from 18.2% to 19.8%, with the PCE of the best device found to be 21% when 3% PS was used (Figure 3d, Figures S4 and S5, and Table S1). However, this approach might not be able to remove hysteresis issues in current density–voltage (J–V) characteristics although the fill factor in a reverse-to-forward bias sweep was enhanced compared to the one from the control device (Figure S6 and Table S1). Nevertheless, the PS-treated solar cell shows a reduced chemical capacitance (Figure S7) which implies that capacitive hysteresis should be reduced accordingly. Considering the experimental result, the limitation of FF enhancement in a reverse-to-forward bias sweep might be attributed to another

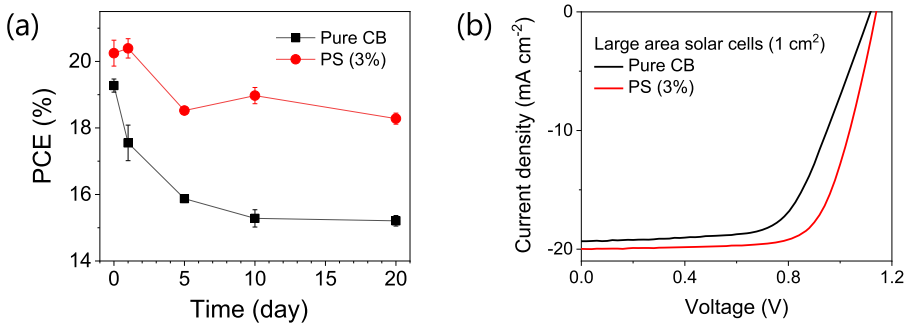

Figure 5. (a) Long-term stability test results of perovskite films in air (RH ≈ 20%, $T \approx 80$ °C). (b) J–V characteristics of large area solar cells processed with and without polymer-capped solvent annealing, respectively.

source such as a noncapacitive hysteresis, which could occur due to an interfacial modification and/or a contact reactivity caused by perovskite ionic motions and/or halide vacancies. Thus, this type of hysteresis should be targeted with different approaches such as alkali metal cation (e.g., K^+) addition in the bulk and/or alkali metal cation treatment on an electron transport layer (ETL),[30−32] which is beyond the scope of our study. Therefore, a follow-up study using a potassium treatment together with our polymer-capped solvent annealing or changing the device structure to the p−i−n architecture might be needed to see if both the energetic disorder and the halide vacancies could be controlled simultaneously.

To elucidate the impact of the polymer-capped solvent-annealing process on the solar cell parameters, we further analyzed the solar cell processed with 3% PS solution which exhibited the highest values for the PCE and FF. We compare photoluminescence (PL) data, which show a peak shift to shorter wavelength (762 to 758 nm) and narrower fwhm (46 to 44.7 nm) upon the PS-capped solvent-annealing process (Figure 4a and Figure S8a). Tauc plots also show shifts in absorption onsets to higher energies (1.579−1.583 eV) along with sharper slopes (Figure S8b). These results may imply that the smeared-out band edge recedes from the band gap to some extent, which could be due to reduction in energetic disorder in the solar cells.[33] To support this postulation, we characterized the energetic disorder in the solar cells by measuring the distribution of the electronic density of states (DOS). To do this, we extracted chemical capacitance (C_μ) using a widely used equivalent circuit for planar heterojunction perovskite solar cells (Figure S7a).[34−38] The C_μ at open-circuit condition, under different light intensities, reflects the density of occupied charge carriers at each quasi-Fermi level in the solar cells. This method can therefore be used to record the variation in the DOS near the band edges. We fit the DOS with either a Gaussian or an Urbach tail (Figure 4b).[37−39] Detailed descriptions for both can be found in the experimental section and SI (Figure S7b). From the Gaussian fit, the width of distribution (or degree of energetic disorder) is found to decrease from 121 to 62 meV upon the polymer-capped solvent annealing with 3% PS. From the Urbach tail fitting, the characteristic energy decreased from 71 to 44 eV. Since both characteristic figures could represent the distributions of gap states near the band edges, the reduction in either energy could reflect the recession of smeared-out band edge, which is a likely cause for the observed V_{OC} enhancement.

The less disordered perovskite layer seems to have less trap-induced recombination. Figure 4c shows the V_{OC} variation as a function of the light intensity, which is an indicator for the degree of trap-assisted recombination in the device.[40] If the slope of the plot is closer to 2, there is a dominant trap-assisted recombination in the solar cells.[41] On the other hand, when it is less than 2, it infers that trap-assisted recombination is suppressed.[11] In Figure 4c, the 3% PS-treated perovskite solar cell shows a lower slope ($1.19\ k_BTq^{-1}$) than that of pure-CB-treated perovskite solar cell ($1.41\ k_BTq^{-1}$). Hence, it could be expected that the polymer-capped solvent-annealing process suppresses trap-assisted recombination. Furthermore, the fill factor is mainly affected by carrier recombination. Therefore, the polymer-capped solvent-annealing process might reduce the energetic disorder as well as trap-assisted recombination in the solar cell, resulting in a high V_{OC} and FF.

When we plot the FF as a function of V_{OC}, a significant improvement in ideality factor is observed upon the polymer-capped solvent-annealing process. By adopting an equation from traditional inorganic p−n junction solar cells,[42,43] we can express FF as

$$\mathrm{FF} = \frac{\tilde{v}_{oc} - \ln(\tilde{v}_{oc} + 0.72)}{\tilde{v}_{oc} + 1} \quad (1)$$

where $\tilde{v}_{oc}$ is the V_{OC} normalized to the thermal voltage,

$$\tilde{v}_{oc} = \frac{V_{OC}}{n_{id}kT/q} \quad (2)$$

k is the Boltzmann constant, T is temperature, q is the elementary charge, and n_{id} is an ideality factor which is related to a characteristic diode behavior; as n_{id} is approaching unity, the diode becomes ideally operating.[44] In Figure 4d, it is found that a crossing point of the V_{OC} and FF for the control solar cell is lying between n_{id} = 2.0 and 2.5, whereas, for the polymer-capped solvent-annealed solar cell, it is located at n_{id} = 1.5. Therefore, the polymer-capped solvent-annealing process might facilitate a better solar cell operation by reducing disorder and recombination in the solar cells.

To investigate the stability of the perovskite films, without any direct influence of the back-contacts, we prepared two batches of films: one batch with films treated with pure CB and the other batch with films treated with the 3% PS solution. Each batch contained five sets of films, each containing 3 cells (30 cells in total), that were designed to be exposed to air (RH ≈ 20%, $T \approx$ 80 °C) for 0, 1, 5, 10, and 20 days, respectively. Before exposing the perovskite films to air, all of the PS-treated perovskite films were washed with CB to remove the entirety of the PS and were subsequently dried with N_2. Because LiTFSI, which is normally used as a dopant to the spiro-OMeTAD hole-transport layer, can negatively affect device stability, we performed the aging process before completing the full solar cell architecture, i.e., before

processing the hole-transport layer and Au electrode. After certain periods of exposure time, the spiro-OMeTAD and Au electrode were deposited on the aged perovskite films, and completely fabricated solar cells were tested. As shown in Figure 5a, the PCEs for the control films treated with CB decreased by more than 20% after 20-day air-exposure, whereas the PCEs for the PS-capped solvent-annealed films decreased by less than 10% during the same period of time (Figure 5a). Notably, the efficiency difference between the two groups is significantly widened from 5% to more than 20% after 20 days of air exposure. The slow reduction in PCE for the PS-capped solvent-annealed samples might be attributed to the reduced reactive area of the grain boundaries and the enhanced crystallite sizes.[45,46] Moreover, the PS-capped solvent-annealing process might be beneficial for the large area solar cell fabrication since this technique renders the surface of the perovskite layer flatter (Figure S1). In large area solar cells and modules, a single pinhole may cause the entire cell to shunt, which dramatically reduces the device performance or could even lead to device failure.[47] In our large area solar cells with the active area = 1 cm^2 the PCEs from the PS-treated solar cells are higher than those of the control cells treated with CB, further exhibiting a narrower PCE deviation (Figure 5b and Table S2). The smooth and flat perovskite films (Figure S1) may also facilitate better contact with the spiro-OMeTAD layer, preventing pinholes and physical defects at the interface.[47,48]

In summary, we demonstrate that a polymer-capped solvent-annealing process assisted by a hot air blower suppresses the occurrence of δ-phase perovskites and simultaneously increases the crystallite size of α-phase perovskites, possibly leading to less trap-assisted recombination and lower energetic disorder of the solar cells. Thus, the polymer-capped solvent-annealed solar cells exhibit FFs as high as 85% with an enhanced V_{OC} of up to 1.15 V without sacrificing any J_{SC}. In addition, the compactly packed clusters of the perovskite grains reduce the degree of degradation, making the solar cells stable in air over a duration of 20 days. Moreover, the flat perovskite layer surface which was induced by the PS film is beneficial for the large area solar cell fabrication with high reliability. Our approach and results show great potential for further efficiency improvements and could be widely used to control the grain/crystallite size of a polycrystalline perovskite layer for optoelectronic devices.

■ ASSOCIATED CONTENT

Supporting Information

The Supporting Information is available free of charge at https://pubs.acs.org/doi/10.1021/acsaem.0c00854.

Experimental methods, AFM topology images, polarization modulation−infrared reflection absorption spectroscopy, cross-sectional SEM images, EQE, time-dependent power density at the voltage of maximum power output, equivalent circuit of IS response and chemical capacitance plot, photoluminescence and Tauc plot, and tables (PDF)

■ AUTHOR INFORMATION

Corresponding Author

André D. Taylor − *Department of Chemical and Biomolecular Engineering, New York University Tandon School of Engineering, Brooklyn, New York 11201, United States; Department of Chemical and Environmental Engineering, Yale University, New Haven, Connecticut 06511, United States;* orcid.org/0000-0003-3241-8543; Email: andre.taylor@nyu.edu

Authors

Jaemin Kong − *Department of Chemical and Biomolecular Engineering, New York University Tandon School of Engineering, Brooklyn, New York 11201, United States; Department of Chemical and Environmental Engineering, Yale University, New Haven, Connecticut 06511, United States;* orcid.org/0000-0002-3236-1658

Hanyu Wang − *Department of Chemical and Environmental Engineering, Yale University, New Haven, Connecticut 06511, United States;* orcid.org/0000-0003-2170-4536

Jason A. Röhr − *Department of Chemical and Biomolecular Engineering, New York University Tandon School of Engineering, Brooklyn, New York 11201, United States*

Zachary S. Fishman − *Department of Chemical and Environmental Engineering, Yale University, New Haven, Connecticut 06511, United States*

Yuanyuan Zhou − *School of Engineering, Brown University, Providence, Rhode Island 02912, United States*

Mingxing Li − *Center for Functional Nanomaterials, Brookhaven National Laboratory, Upton, New York 11973, United States*

Mircea Cotlet − *Center for Functional Nanomaterials, Brookhaven National Laboratory, Upton, New York 11973, United States*

Geunjin Kim − *Division of Advanced Materials, Korea Research Institute of Chemical Technology (KRICT), Daejeon 34114, South Korea*

Christopher Karpovich − *Department of Chemical and Environmental Engineering, Yale University, New Haven, Connecticut 06511, United States*

Francisco Antonio − *Department of Chemical and Environmental Engineering, Yale University, New Haven, Connecticut 06511, United States*

Nitin P. Padture − *School of Engineering, Brown University, Providence, Rhode Island 02912, United States;* orcid.org/0000-0001-6622-8559

Complete contact information is available at: https://pubs.acs.org/10.1021/acsaem.0c00854

Notes

The authors declare no competing financial interest.

■ ACKNOWLEDGMENTS

We gratefully acknowledge the National Science Foundation NSF-PECASE award (CBET-0954985) and New York University for partial support of this work. The Yale Institute for Nanoscience and Quantum Engineering (YINQE) and NSF MRSEC DMR 1119826 (CRISP) provided facility support. The research at Brown University was performed under the funding support from the National Science Foundation (Grants OIA-1538893 and OIA-1929019) and Office for Naval Research (Grant N00014-17-1-2232 and N00014-20-1-2574). The research used resources of the Center for Functional Nanomaterials, which is a U.S. DOE Office of Science Facility, at Brookhaven National Laboratory under Contract No. DE-SC0012704. We thank Jacob A. Spies for fruitful discussions.

■ REFERENCES

(1) Kojima, A.; Teshima, K.; Shirai, Y.; Miyasaka, T. Organometal halide perovskites as visible-light sensitizers for photovoltaic cells. *J. Am. Chem. Soc.* **2009**, *131* (17), 6050−1.

(2) Yang, Z.; Surrente, A.; Galkowski, K.; Bruyant, N.; Maude, D. K.; Haghighirad, A. A.; Snaith, H. J.; Plochocka, P.; Nicholas, R. J. Unraveling the Exciton Binding Energy and the Dielectric Constant in Single-Crystal Methylammonium Lead Triiodide Perovskite. *J. Phys. Chem. Lett.* **2017**, *8* (8), 1851−1855.
(3) Stranks, S. D.; Eperon, G. E.; Grancini, G.; Menelaou, C.; Alcocer, M. J. P.; Leijtens, T.; Herz, L. M.; Petrozza, A.; Snaith, H. J. Electron-Hole Diffusion Lengths Exceeding 1 Micrometer in an Organometal Trihalide Perovskite Absorber. *Science* **2013**, *342* (6156), 341−344.
(4) National Renewable Energy Laboratory (NREL). *Best Research Cell Efficiencies*; https://www.nrel.gov/pv/cell-efficiency.html (accessed 2019-09-10).
(5) Shockley, W.; Queisser, H. J. Detailed Balance Limit of Efficiency of p-n Junction Solar Cells. *J. Appl. Phys.* **1961**, *32* (3), 510−519.
(6) Sha, W. E. I.; Ren, X. G.; Chen, L. Z.; Choy, W. C. H. The efficiency limit of CH3NH3PbI3 perovskite solar cells. *Appl. Phys. Lett.* **2015**, *106* (22), 221104.
(7) Ruhle, S. Tabulated values of the Shockley-Queisser limit for single junction solar cells. *Sol. Energy* **2016**, *130*, 139−147.
(8) Bi, D. Q.; Tress, W.; Dar, M. I.; Gao, P.; Luo, J. S.; Renevier, C.; Schenk, K.; Abate, A.; Giordano, F.; Correa Baena, J.-P.; Decoppet, J. D.; Zakeeruddin, S. M.; Nazeeruddin, M. K.; Gratzel, M.; Hagfeldt, A. Efficient luminescent solar cells based on tailored mixed-cation perovskites. *Sci. Adv.* **2016**, *2* (1), e1501170.
(9) Yang, W. S.; Park, B. W.; Jung, E. H.; Jeon, N. J.; Kim, Y. C.; Lee, D. U.; Shin, S. S.; Seo, J.; Kim, E. K.; Noh, J. H.; Seok, S. I. Iodide management in formamidinium-lead-halide-based perovskite layers for efficient solar cells. *Science* **2017**, *356* (6345), 1376−1379.
(10) Jung, E. H.; Jeon, N. J.; Park, E. Y.; Moon, C. S.; Shin, T. J.; Yang, T. Y.; Noh, J. H.; Seo, J. Efficient, stable and scalable perovskite solar cells using poly(3-hexylthiophene). *Nature* **2019**, *567* (7749), 511−515.
(11) Sherkar, T. S.; Momblona, C.; Gil-Escrig, L.; Avila, J.; Sessolo, M.; Bolink, H. J.; Koster, L. J. A. Recombination in Perovskite Solar Cells: Significance of Grain Boundaries, Interface Traps, and Defect Ions. *Acs Energy Lett.* **2017**, *2* (5), 1214−1222.
(12) Wang, F.; Bai, S.; Tress, W.; Hagfeldt, A.; Gao, F. Defects engineering for high-performance perovskite solar cells. *npj Flexible Electronics* **2018**, *2* (1), 22.
(13) Tang, X. F.; van den Berg, M.; Gu, E. N.; Horneber, A.; Matt, G. J.; Osvet, A.; Meixner, A. J.; Zhang, D.; Brabec, C. J. Local Observation of Phase Segregation in Mixed-Halide Perovskite. *Nano Lett.* **2018**, *18* (3), 2172−2178.
(14) McKenna, K. P. Electronic Properties of {111} Twin Boundaries in a Mixed-Ion Lead Halide Perovskite Solar Absorber. *Acs Energy Lett.* **2018**, *3* (11), 2663−2668.
(15) Bi, D. Q.; Yi, C. Y.; Luo, J. S.; Decoppet, J. D.; Zhang, F.; Zakeeruddin, S. M.; Li, X.; Hagfeldt, A.; Gratzel, M. Polymer-templated nucleation and crystal growth of perovskite films for solar cells with efficiency greater than 21%. *Nat. Energy* **2016**, *1*, 16142.
(16) Zhang, F.; Shi, W. D.; Luo, J. S.; Pellet, N.; Yi, C. Y.; Li, X.; Zhao, X. M.; Dennis, T. J. S.; Li, X. G.; Wang, S. R.; Xiao, Y.; Zakeeruddin, S. M.; Bi, D. Q.; Gratzel, M. Isomer-Pure Bis-PCBM-Assisted Crystal Engineering of Perovskite Solar Cells Showing Excellent Efficiency and Stability. *Adv. Mater.* **2017**, *29* (17), 1606806.
(17) Li, F. C.; Yuan, J. Y.; Ling, X. F.; Zhang, Y. N.; Yang, Y. G.; Cheung, S. H.; Ho, C. H. Y.; Gao, X. Y.; Ma, W. L. A Universal Strategy to Utilize Polymeric Semiconductors for Perovskite Solar Cells with Enhanced Efficiency and Longevity. *Adv. Funct. Mater.* **2018**, *28* (15), 1706377.
(18) Wu, Y. H.; Wang, P.; Wang, S. B.; Wang, Z. H.; Cai, B.; Zheng, X. J.; Chen, Y.; Yuan, N. Y.; Ding, J. N.; Zhang, W. H. Heterojunction Engineering for High Efficiency Cesium Formamidinium Double-Cation Lead Halide Perovskite Solar Cells. *ChemSusChem* **2018**, *11* (5), 837−842.
(19) Li, X.; Li, W.; Yang, Y.; Lai, X.; Su, Q.; Wu, D.; Li, G.; Wang, K.; Chen, S.; Sun, X. W.; Kyaw, A. K. K. Defects Passivation With Dithienobenzodithiophene-based π-conjugated Polymer for Enhanced Performance of Perovskite Solar Cells. *Solar RRL* **2019**, *3* (6), 1900029.
(20) Zhang, H. Y.; Shi, J. J.; Zhu, L. F.; Luo, Y. H.; Li, D. M.; Wu, H. J.; Meng, Q. B. Polystyrene stabilized perovskite component, grain and microstructure for improved efficiency and stability of planar solar cells. *Nano Energy* **2018**, *43*, 383−392.
(21) Li, M. H.; Yan, X. Q.; Kang, Z.; Huan, Y. H.; Li, Y.; Zhang, R. X.; Zhang, Y. Hydrophobic Polystyrene Passivation Layer for Simultaneously Improved Efficiency and Stability in Perovskite Solar Cells. *ACS Appl. Mater. Interfaces* **2018**, *10* (22), 18787−18795.
(22) Huang, J. S.; Goh, T.; Li, X. K.; Sfeir, M. Y.; Bielinski, E. A.; Tomasulo, S.; Lee, M. L.; Hazari, N.; Taylor, A. D. Polymer bulk heterojunction solar cells employing Forster resonance energy transfer. *Nat. Photonics* **2013**, *7* (6), 479−485.
(23) Goh, T.; Huang, J. S.; Bartolome, B.; Sfeir, M. Y.; Vaisman, M.; Lee, M. L.; Taylor, A. D. Panchromatic polymer-polymer ternary solar cells enhanced by Forster resonance energy transfer and solvent vapor annealing. *J. Mater. Chem. A* **2015**, *3* (36), 18611−18621.
(24) Binek, A.; Hanusch, F. C.; Docampo, P.; Bein, T. Stabilization of the Trigonal High-Temperature Phase of Formamidinium Lead Iodide. *J. Phys. Chem. Lett.* **2015**, *6* (7), 1249−1253.
(25) Ono, L. K.; Juarez-Perez, E. J.; Qi, Y. B. Progress on Perovskite Materials and Solar Cells with Mixed Cations and Halide Anions. *ACS Appl. Mater. Interfaces* **2017**, *9* (36), 30197−30246.
(26) Yun, J. S.; Kim, J.; Young, T.; Patterson, R. J.; Kim, D.; Seidel, J.; Lim, S.; Green, M. A.; Huang, S. J.; Ho-Baillie, A. Humidity-Induced Degradation via Grain Boundaries of HC(NH2)(2)PbI3 Planar Perovskite Solar Cells. *Adv. Funct. Mater.* **2018**, *28* (11), 1705363.
(27) Cordero, F.; Craciun, F.; Trequattrini, F.; Generosi, A.; Paci, B.; Paoletti, A. M.; Pennesi, G. Stability of Cubic FAPbI(3) from X-ray Diffraction, Anelastic, and Dielectric Measurements. *J. Phys. Chem. Lett.* **2019**, *10* (10), 2463−2469.
(28) Liu, T. H.; Zong, Y. X.; Zhou, Y. Y.; Yang, M. J.; Li, Z.; Game, O. S.; Zhu, K.; Zhu, R.; Gong, Q. H.; Padture, N. P. High-Performance Formamidinium-Based Perovskite Solar Cells via Microstructure-Mediated delta-to-alpha Phase Transformation. *Chem. Mater.* **2017**, *29* (7), 3246−3250.
(29) Kim, G. W.; Shinde, D. V.; Park, T. Thickness of the hole transport layer in perovskite solar cells: performance versus reproducibility. *RSC Adv.* **2015**, *5* (120), 99356−99360.
(30) Bu, T. L.; Li, J.; Zheng, F.; Chen, W. J.; Wen, X. M.; Ku, Z. L.; Peng, Y.; Zhong, J.; Cheng, Y. B.; Huang, F. Z. Universal passivation strategy to slot-die printed SnO2 for hysteresis-free efficient flexible perovskite solar module. *Nat. Commun.* **2018**, *9*, 4609.
(31) Kang, D. H.; Park, N. G. On the Current-Voltage Hysteresis in Perovskite Solar Cells: Dependence on Perovskite Composition and Methods to Remove Hysteresis. *Adv. Mater.* **2019**, *31* (34), 1805214.
(32) Abdi-Jalebi, M.; Andaji-Garmaroudi, Z.; Cacovich, S.; Stavrakas, C.; Philippe, B.; Richter, J. M.; Alsari, M.; Booker, E. P.; Hutter, E. M.; Pearson, A. J.; Lilliu, S.; Savenije, T. J.; Rensmo, H.; Divitini, G.; Ducati, C.; Friend, R. H.; Stranks, S. D. Maximizing and stabilizing luminescence from halide perovskites with potassium passivation. *Nature* **2018**, *555* (7697), 497−501.
(33) Shao, Y. H.; Xiao, Z. G.; Bi, C.; Yuan, Y. B.; Huang, J. S. Origin and elimination of photocurrent hysteresis by fullerene passivation in CH3NH3PbI3 planar heterojunction solar cells. *Nat. Commun.* **2014**, *5*, 5784.
(34) Xiao, Z.; Dong, Q.; Bi, C.; Shao, Y.; Yuan, Y.; Huang, J. Solvent Annealing of Perovskite-Induced Crystal Growth for Photovoltaic-Device Efficiency Enhancement. *Adv. Mater.* **2014**, *26* (37), 6503−6509.
(35) Deng, Y. H.; Peng, E.; Shao, Y. C.; Xiao, Z. G.; Dong, Q. F.; Huang, J. S. Scalable fabrication of efficient organolead trihalide perovskite solar cells with doctor-bladed active layers. *Energy Environ. Sci.* **2015**, *8* (5), 1544−1550.
(36) Contreras-Bernal, L.; Ramos-Terrón, S.; Riquelme, A.; Boix, P. P.; Idígoras, J.; Mora-Seró, I.; Anta, J. A. Impedance analysis of perovskite solar cells: a case study. *J. Mater. Chem. A* **2019**, *7* (19), 12191−12200.

(37) Bisquert, J. Interpretation of electron diffusion coefficient in organic and inorganic semiconductors with broad distributions of states. *Phys. Chem. Chem. Phys.* **2008**, *10* (22), 3175−3194.
(38) Shao, Y. C.; Yuan, Y. B.; Huang, J. S. Correlation of energy disorder and open-circuit voltage in hybrid perovskite solar cells. *Nat. Energy* **2016**, *1*, 15001.
(39) Urbach, F. The Long-Wavelength Edge of Photographic Sensitivity and of the Electronic Absorption of Solids. *Phys. Rev.* **1953**, *92* (5), 1324−1324.
(40) Nie, W. Y.; Tsai, H. H.; Asadpour, R.; Blancon, J. C.; Neukirch, A. J.; Gupta, G.; Crochet, J. J.; Chhowalla, M.; Tretiak, S.; Alam, M. A.; Wang, H. L.; Mohite, A. D. High-efficiency solution-processed perovskite solar cells with millimeter-scale grains. *Science* **2015**, *347* (6221), 522−525.
(41) Koster, L. J. A.; Mihailetchi, V. D.; Ramaker, R.; Blom, P. W. M. Light intensity dependence of open-circuit voltage of polymer:fullerene solar cells. *Appl. Phys. Lett.* **2005**, *86* (12), 123509.
(42) Green, M. A. Solar-Cell Fill Factors - General Graph and Empirical Expressions. *Solid-State Electron.* **1981**, *24* (8), 788−789.
(43) Guo, X. G.; Zhou, N. J.; Lou, S. J.; Smith, J.; Tice, D. B.; Hennek, J. W.; Ortiz, R. P.; Navarrete, J. T. L.; Li, S. Y.; Strzalka, J.; Chen, L. X.; Chang, R. P. H.; Facchetti, A.; Marks, T. J. Polymer solar cells with enhanced fill factors. *Nat. Photonics* **2013**, *7* (10), 825−833.
(44) Li, X.; Huang, J. S.; Nejati, S.; McMillon, L.; Huang, S.; Osuji, C. O.; Hazari, N.; Taylor, A. D. Role of HF in Oxygen Removal from Carbon Nanotubes: Implications for High Performance Carbon Electronics. *Nano Lett.* **2014**, *14* (11), 6179−6184.
(45) Fei, C. B.; Li, B.; Zhang, R.; Fu, H. Y.; Tian, J. J.; Cao, G. Z. Highly Efficient and Stable Perovskite Solar Cells Based on Monolithically Grained CH3NH3PbI3 Film. *Adv. Energy Mater.* **2017**, *7* (9), 1602017.
(46) Chu, Z. D.; Yang, M. J.; Schulz, P.; Wu, D.; Ma, X.; Seifert, E.; Sun, L. Y.; Li, X. Q.; Zhu, K.; Lai, K. J. Impact of grain boundaries on efficiency and stability of organic-inorganic trihalide perovskites. *Nat. Commun.* **2017**, *8*, 2230.
(47) Deng, Y. H.; Zheng, X. P.; Bai, Y.; Wang, Q.; Zhao, J. J.; Huang, J. S. Surfactant-controlled ink drying enables high-speed deposition of perovskite films for efficient photovoltaic modules. *Nat. Energy* **2018**, *3* (7), 560−566.
(48) Kim, D. H.; Whitaker, J. B.; Li, Z.; van Hest, M. F. A. M.; Zhu, K. Outlook and Challenges of Perovskite Solar Cells toward Terawatt-Scale Photovoltaic Module Technology. *Joule* **2018**, *2* (8), 1437−1451.